

# A Novel Method for Real Time Protection of DC Microgrid Using Cumulative Summation and Wavelet Transform

Original Scientific Paper

## Dipti D Patil

Department of Electrical Engineering, Fr. C. Rodrigues Institute of Technology  
Navi Mumbai, Maharashtra, India  
diptipatil009@gmail.com

## Bindu S

Department of Electrical Engineering, Fr. C. Rodrigues Institute of Technology  
Navi Mumbai, Maharashtra, India  
bindu.s@fcrit.ac.in

## Sushil Thale

Department of Electrical Engineering, Fr. C. Rodrigues Institute of Technology  
Navi Mumbai, Maharashtra, India  
sushil.thale@fcrit.ac.in

**Abstract** – DC microgrid is a compact framework comprising interconnected nearby sources and loads. The renewable energy source used in DC microgrids being intermittent leads to the change in the power availability as well as the fault current levels. In such situations, detecting and clearing the faults is very important to protect the DC microgrid without compromising on fault clearing time and interruption of the load. This paper proposes a hybrid Cumulative Sum (CumSum) and Wavelet transform-based approach to detect the fault. The CumSum value raises the amplitude by averaging the fault current. Wavelet transforms obtain important fault current features by decomposing the current signal. The hybrid method of CumSum and Wavelet analysis proposed here enables the detection of the fault and differentiates the fault condition from sudden load variation. Additionally, it helps to recognize the location of the fault by the wavelet energy difference. The proposed scheme is tested with a developed ring-type low voltage DC (LVDC) microgrid hardware model under various fault conditions. The scheme is implemented using TMS320F28069 digital signal processors (DSP) of Texas Instruments. The hardware results are validated using MATLAB simulation. The proposed method performance is also compared with the existing methods used for DC microgrid protection. The outcome shows that the proposed method has a high accuracy of 98.72%, selectivity of 96.08%, and reliability of 99.01%. The execution time required by the proposed method is also less.

---

**Keywords:** Fault Detection and protection, DC microgrid, CumSum, Wavelet Transform.

---

## 1. INTRODUCTION

The microgrid (MG) is a rising and most encouraging idea in both AC and DC systems. It can be mainly classified into AC, DC, or a mix of both i.e. hybrid. The microgrid comprises the small interconnection of local distributed renewable and non-renewable sources and loads. Such a structure is efficient for working in one islanded and the other grid-associated modes [1]. A microgrid provides a reliable and high-power quality electric supply as well [2]. In a DC microgrid, a large portion of the sustainable power sources are DC sources like solar, fuel cell, and so on that can supply to the DC load directly. Hence eliminating the con-

version stages and improving the overall system efficiency. Control requirements are also reduced in DC microgrids because of the absence of reactive power control and frequency synchronization as compared to the AC microgrid [3]. However, along with these benefits, microgrids have also raised several challenges like high installation cost and protection issues, and low system inertia [4]. Because of the discontinuous type of the sources, low fault levels, and switching structure arrangement, protection becomes one of the significant difficulties in a microgrid. This poses a constraint on the fault detection time and isolation of the healthy part. Also, in the AC system, fault location is identified from the variation of impedance. In the case of DC structure,

fault impedance is not the same as that of the AC structure because of the smaller length of the lines and thus identification of the exact location of the fault is additionally a difficult issue [5]. In DC microgrid sources and load are connected through power electronic converters. These converters are operated in voltage control mode or current control mode to maintain the output power constant. The output of the power converter on the load side is constant. Therefore a reduction in voltage of the power converter leads to an increase in load current which results in oscillations in voltage and current [6]. In the case of standalone operation of DC microgrid, the fault current is low, it will become difficult to protection devices to distinguish between oscillation due to fault scenario or oscillation due to constant power operation of the converter.

Adaptive protection of the distribution system is proposed by Mahat, *et al.* using directional overcurrent relays. Relays have fixed commanding attributes for grid-associated and island conditions and operate only for the forward direction of the fault current [7]. A power probe unit equipped with a non-iterative strategy was proposed to find fault position for LVDC microgrid. However, this technique utilizes additional instruments to estimate the DC fault area [8]. Active impedance and a traveling wave-based fault identification technique are the few methods used for DC microgrid for protection [9-10]. Balasreedharan, *et al.*, and Meghawani, *et al.* proposed higher-order derivatives for the detection of the fault but this method is immensely delicate to the noise amount of the signal [11-12]. The current differential protection (CDP) proposed in the literature requires communication devices that increase the weight size and cost of the system. Anyways, the ongoing improvement of the smart grid extends the provision for the incorporation of a more particular, communication-based, protection strategy that uses this high-level infrastructure. Also, the output of the current transducer used for DC measurement is the voltage which allows an effortless combination with digital processing devices [13]. Recently, most of the research that relied on time frequency analysis to find the fault features and these features are as attributes to learn and build classifier model. This classifier model was then used for detection and classification of faults. However, the performance of the classifier model, which was based on time frequency analysis, was significantly affected by the computational complexity and time of technique [14]. Deep neural network enabled fault detection in LVDC microgrid using empirical mode decomposition (EMD) is proposed by Dipti *et al.* In this paper EMD extracts the characteristics of the fault signal and these extracted features are utilized at the time of training of the Convolutional neural network (CNN). The trained network is then utilised to classify the normal, abnormal and fault condition in LVDC microgrid. [15].

DC microgrid fault current level undergoes enormous alteration because of the uncertain characteristics of the intermittent sources, changes in network topology, and

switching on and off of heavy or light load. Therefore, traditional overcurrent protection schemes do not work effectively against the fault in the DC microgrid. Taking the above issues into account, the contribution of the proposed exploration method related to DC microgrid protection is differentiating between system dynamics and fault scenario, the quick discovery of the fault, and the disconnection of the defective segment to protect healthy sections from high fault current surge. As well as a similar procedure can be utilized to recognize the specific area of a fault. A real-time fault identification technique using Cumulative Sum and wavelet-based characteristics extraction of fault current wave in a DC microgrid is proposed in this paper. This paper likewise features the fault location identification from the Energy per cycle of the wavelet coefficient.

The paper is coordinated as follows; an audit of existing protection techniques for the microgrid is accounted for in section 1. Possible fault in the DC microgrid and fault current behavior is presented in section 2. Wavelet-based fault detection and localization using fault current features and calculation of the cumulative sum of fault current are explained in section 3. The Proposed fault detection algorithm using *CumSum* average, wavelet transform analysis and threshold setting is presented in the section. 4. The development of a lab model of an LVDC microgrid is presented in section 5. The suggested protection scheme is tested on hardware and results are discussed in section 6. Hardware results are approved using simulation results under different fault situations are presented in section 7 followed by the conclusion in section 8.

## 2. DC MICROGRID FAULT ANALYSIS

DC Bus to bus and bus to ground faults mainly occur in the DC microgrid system. When the positive and negative bus comes in contact, it creates a direct short-circuit fault or bus to bus fault and when the positive or negative bus comes in contact with the ground, it develops the bus to ground fault. In a DC microgrid bus to bus fault is the major serious fault for the converter. As a power electronic converter can be obstructed for self-security during faults; it allows reverse diodes of the device to be exposed to a fault [16]. A bus-to-bus fault in the DC segment may be responsible for peak transient fault current because of charged capacitors and the short impedance of the segment. Figure 1 is the equivalent circuit representation of the DC segment under fault conditions. Voltage source converter ( $V_{sc}$ ) is the voltage source converter connected across the source. The notations  $r$  and  $L$  are used to represent the resistance and inductance of the segment. Filter capacitance is represented by notation  $C$  and  $R_f$  as well as  $I_f$  are the fault resistance and fault current respectively. During the bus to bus fault, the capacitor starts discharging through the segment impedance of the source to bus fault the point ( $R = r + R_f$  and  $L$ ).

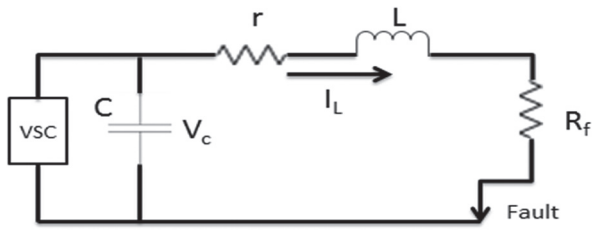


**Fig. 1.** RLC Equivalent fault circuit

$$i(s) = \frac{V_c(0)}{L} + \frac{i_L(0)s}{s^2 + \frac{R}{L}s + \frac{1}{LC}} \quad (1)$$

Where,  $V_c(0)$  is the voltage across the capacitor and  $i_L(0)$  is the current through the inductor just before the occurrence of fault. The equation of fault current in time domain is

$$i(t) = \frac{V_c(0)}{L(S_2 - S_1)} [e^{-S_1 t} - e^{-S_2 t}] + \frac{i_L(0)}{S_2 - S_1} [-S_1 e^{-S_1 t} + S_2 e^{-S_2 t}] \quad (2)$$

where

$$S_1, S_2 = \frac{R}{2L} \pm \sqrt{\left(\frac{R}{2L}\right)^2 - \left(\frac{1}{LC}\right)} \quad (3)$$

$$S_1, S_2 = \alpha \pm \sqrt{(\alpha)^2 - (\omega_0)^2} \quad (4)$$

Where  $\alpha$  is the attenuation and  $\omega_0$  is the damped resonant frequency of the fault current.  $S_1$  and  $S_2$  represents the roots of the equation 3. Depending on the value of  $(R/2L)^2$ ,  $(1/LC)$  the values of  $S_1$  and  $S_2$  become real or complex and the fault current response can be over damped, critically damped and under damped. Equation 4 uses notation Hence the rate of oscillation of the fault current relies upon segment parameters  $R$ ,  $L$ , and filter capacitance  $C$  [18].

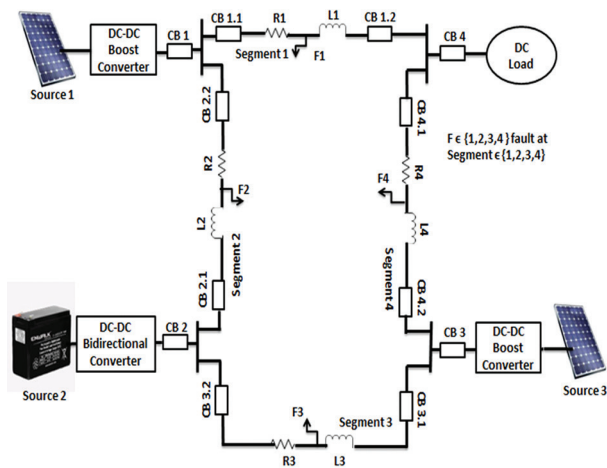


**Fig. 2.** Simulation model for 48 V DC Microgrid

The 48-V dc ring-type architecture shown in Figure 2 with specifications is given in Table II. The DC microgrid model consists of four segments and the length of each segment is taken into an extent of a kilometre.

The system is consisting of four nodes; these nodes are connected with two Renewable Energy Sources (RES), a lead-acid battery bank, and DC electronic load respectively. Each source is interfaced to the microgrid via power electronic converters. (Parameter of converters is same as shown in Table II) Source 1 and source 3 are Solar Photovoltaic (SPV), sources that are interfaced to DC microgrid through a boost converter. The control loop operation of the converter is implemented through the maximum power point tracking (MPPT) controller shown in figure 3. Source 2 is an energy storage system (ESS) source that is interfaced to the DC microgrid through a bi-directional converter. The state of charge (SOC) control loop is executed internally as shown in figure 4. To detect and isolate DC microgrid against fault, relays and circuit breakers are placed at each end of all segments.

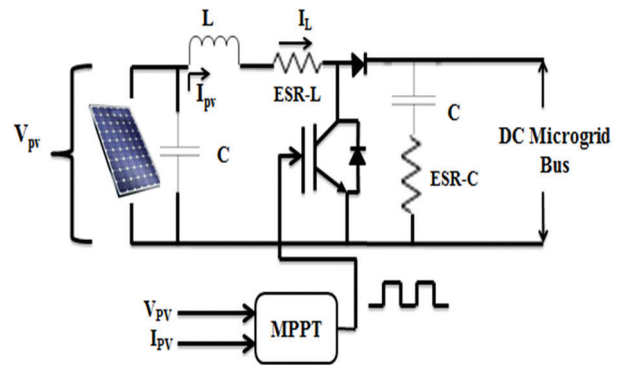


**Fig. 3.** Control schematic of SPV Source 1 and 3 fed DC microgrid via boost converter

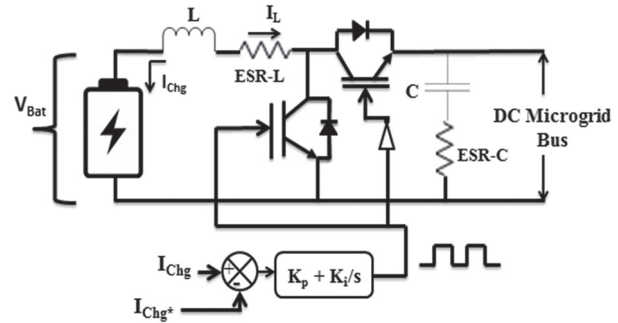


**Fig. 4.** Control schematic of Battery Source 2 fed DC microgrid via bidirectional converter

The fault is created in segment 1 at 10% and 90% distance of the 1-km bus portion with respective source 1. The fault current has a fast-rising transient with a large peak followed by oscillation. The amplitude and oscillation frequency of fault current is different at both distances as it depends on the equivalent parameters of the fault path seen in Figure 5. The distinction of fault current is estimated in the segment by embedding diverse fault resistance (0.1Ω and 0.9Ω) at the half distance of a 1-km bus segment as displayed in Figure 6. The damping effect is marginally high in the case of 0.9 Ω fault resistance compared to 0.1 Ω resistances.

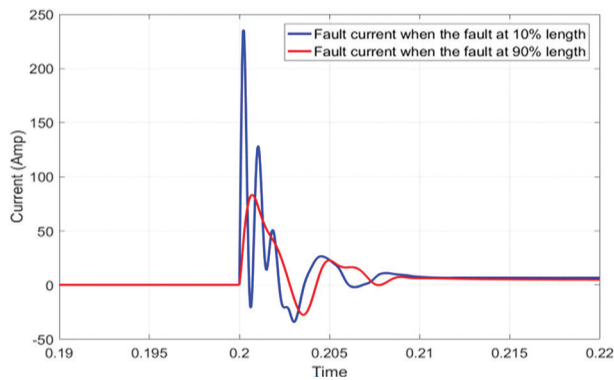


**Fig. 5.** Difference of rate of rise of fault current after the fault is initiated at 10% and 90% distant in segment

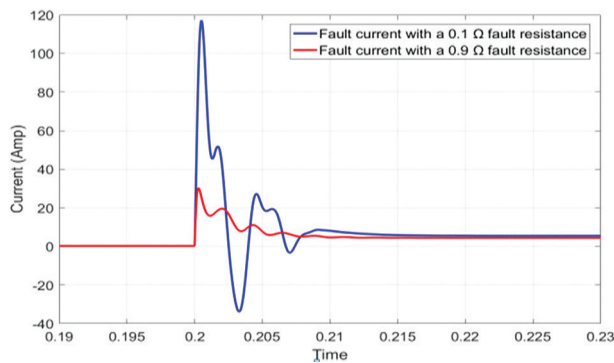


**Fig. 6.** Difference of rate of rise of fault current after the fault is initiated at half distance of a 1-km bus segment with 0.1 Ω and 0.9Ω fault resistance

### 3. PROPOSED FAULT DETECTION AND LOCALISATION METHOD

A hybrid Wavelet and cumulative sum based algorithm is proposed to detect transient and moving average of fault current.

#### 3.1 CUMULATIVE SUMMATION

This technique is a mix of the sample by sample comparison method and moving average cumulative summation (*CumSum*) approach. During the fault condition the segment current changes essentially. For a successful fault detection technique, certain changes should get recognized online with the least noticing samples or time. *CumSum* is based on a moving average calculated by considering 'n' numbers of samples in a window. The average value of summation of n number of samples significantly decreases the computational burden as it uses the simple summation and subtraction operators [19].

*CumSum* = Sum total around the window

$$CumSum = \sum_{k=(t-w)}^t i(k) \quad (5)$$

Where  $t$  is the present time,  $w$  is the window dimension for moving average and  $k$  is a dummy index used for average estimation. The time delay added into the system is  $W$  times the sampling period [20]. The win-

dow size is kept the same as the computational time for the wavelet analysis also. The *CumSum* is a moving average of n number of samples hence, does not affect due to underdamped or overdamped response of fault current. *CumSum* raises the amplitude by averaging the fault current so that the protection relay can detect and isolate the faulty segment [21].

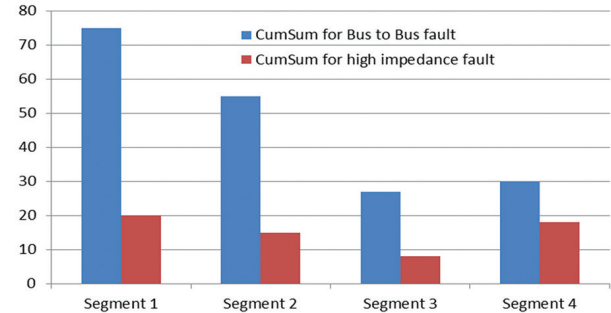


**Fig. 7.** *CumSum* of fault currents in all segments under bus to bus and high impedance fault in segment 1 of Fig. 2.

Figure 7 shows the variation of *CumSum* of fault current in all segments under the bus to bus and high impedance fault (inserted 1 Ω resistance in fault path) at the end of segment 1 of DC microgrid shown in Figure 2. But, the fault in one segment may increase the *CumSum* of current in neighbouring segments, and it can falsely detect as a fault in the neighbouring segment also (mostly observed in high impedance faults). Also a delay in fault detection is observed when more samples are taken for calculating the average.

#### 3.2 WAVELET TRANSFORM

Discrete Wavelet Transform (DWT) calculation is utilized for computerized execution of constant wavelet change utilizing a two-channel perfect reconstruction filter bank. The information signal is disintegrated into low and high-frequency. The high-pass channel relies upon the mother wavelet work, it estimates detail coefficient ( $D_1$ ), and the low pass channel from the scaling capacity of the mother wavelet work estimates approximate coefficients ( $A_1$ ) at the main level [22].

$$A_1(n) = \sum_k h(k - 2n)x(k) \quad (6)$$

$$D_1(n) = \sum_k g(k - 2n)x(k) \quad (7)$$

Here  $h(n)$  is high-pass and  $g(n)$  is a low pass filter coefficient. The input signal is broken down into detail and approximate coefficients through low pass and high pass filters [23]. The subsequent signal is the portrayal of a similar signal in the distinctive frequency groups. Figure 8 shows the wavelet coefficient of fault current in all segments under the bus to bus and high impedance fault (inserted 1 Ω resistance in fault path) at the end of segment 1 of the DC microgrid shown in Figure 2. It is very clear from the bar diagram that the wavelet coefficients of only the faulty segment are much higher than other segment coefficients.

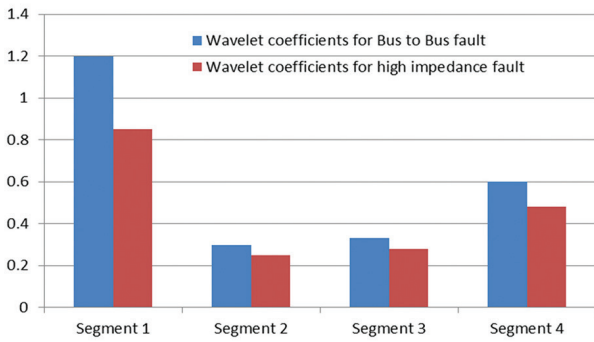


**Fig. 8.** Wavelet coeffs. of fault currents in all segments under bus to bus and high impedance fault in segment 1 (Fig. 2)

However, the dynamics due to a sudden change in load or change in network configuration wavelet analysis gives the magnitude of the same coefficients as that of the magnitude during a fault in the segment. During normal conditions sudden change in load is applied on segment 4 (Figure 2), the load is increased suddenly by 10% of connected load at 0.3 sec. This results in a change in *CumSum* and wavelet coefficient of segment current, it is observed that the wavelet coefficient magnitude is the same as that of the magnitude during a fault in the segment. However, *CumSum* shows only a small variation as shown in Figure 9.

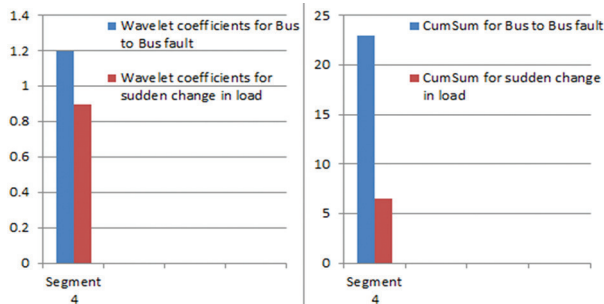


**Fig. 9.** Wavelet coefficients and *CumSum* of current for Bus to Bus fault and after sudden application of load at Segment 4 (Fig 2)

### 3.3 FAULT LOCALISATION

The fault location can be recognized from the current measured from the faulty segment. The sudden variations in the DC system can be analysed as RLC transient conditions due to the resistive, inductive, and capacitive parameters of the DC cable. Wavelet transform decomposes this transient signal with multiple resolutions and gives information about fault current energy concentration in a different band. The energy of the wavelet coefficients usually needs normalization [24].

$$Normalisedd_{ij} = \frac{d_{ij}}{A_{ij}} \quad (8)$$

The energy per cycle from wavelet coefficients [25] is given by

$$E_i = \sum_{j=1}^n Normalised |d_{ij}|^2 \quad (9)$$

Where,  $i$  = Level of the detail coefficient and  $j$  = Samples utilized for each detail coefficient

The detail coefficient extent changes due to the system transients. Consequently; the adjustment of energy demonstrates an unsettling influence in the system. Change in energy is the distinction in energy between two back-to-back cycles it is calculated [26] by equation 10.

$$Change\ in\ Energy = \sqrt{(E_A - E_B)^2} \quad (10)$$

Where,  $E_B$  and  $E_A$  represent the energy of the current cycle and the energy of the past cycle respectively. As the fault location changes the energy concentration value between the start and the endpoint of the segment also changes. This change in energy is used to find the fault location in the segment. Fault near the source causes a high amplitude transient which results in a high wavelet coefficient and higher value of energy. If the fault occurs at the end of the segment amplitude of the transients is low and gives less wavelet high pass coefficient and lesser change in energy value.

### 4. PROPOSED FAULT DETECTION ALGORITHM

The proposed detection method uses two parameters; *CumSum* and wavelet transform. DC Current in the segment is continuously sampled and monitored by the respective current transformer (CTs). *CumSum* and wavelet transform coefficients are calculated from the measured current shown in Figure 10.

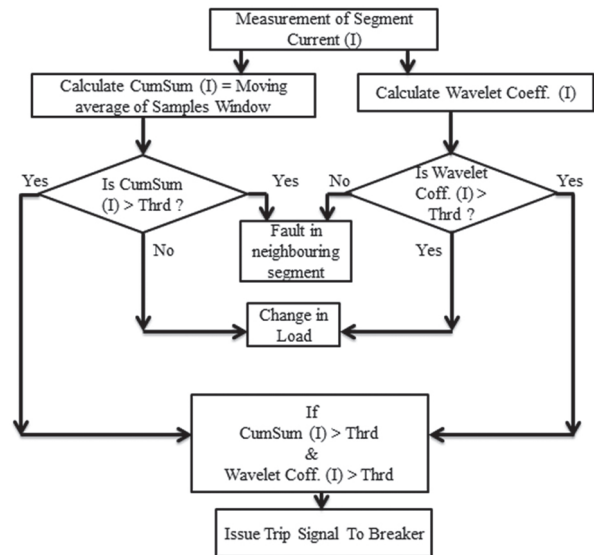


**Fig. 10.** Flow diagram of hybrid protection Scheme

The calculated *CumSum* and wavelet coefficients are compared with the pre-characterized limits of the *CumSum* and wavelet coefficient. The condition, at which the determined *CumSum* and wavelet coefficient are higher than the individual set limit, is distinguished as the fault and a trip signal is initiated to separate the inoperative section from the leftover robust system. If only the *CumSum* of segment current becomes greater than the threshold, it shows a fault in the neighboring segment

and if only calculated wavelet coefficients of segment current become greater than threshold indicates a sudden change in load or network configuration.

**Table 1.** Threshold (*CumSum* and wavelet coefficient) settings for all relays

X	<i>CumSum</i> (Amp) measured at CB(X.1)	Wavelet Coeffs. Measured at CB(X.1)	<i>CumSum</i> (Amp) measured at CB(X.2)	Wavelet Coeffs. Measured at CB(X.2)
1	22	1.4	20	0.9
2	24	0.8	34	6.5
3	20	0.8	34	6.5
4	18	0.9	23	0.8

The threshold of the *CumSum* and wavelet analysis method is determined by initiating fault at the end of the segment with  $1\Omega$  fault resistance one after another. The threshold values obtained by this method are tabulated in Table 1. X is the segment number and it varies from one to four. X.1 indicates the threshold corresponding to one end of the segment and X.2 the other.

## 5. PROTOTYPE OF LVDC MICROGRID

The model of the 48 volts LVDC microgrid is planned and the protection scheme is tested in the hardware setup shown in figure 11.

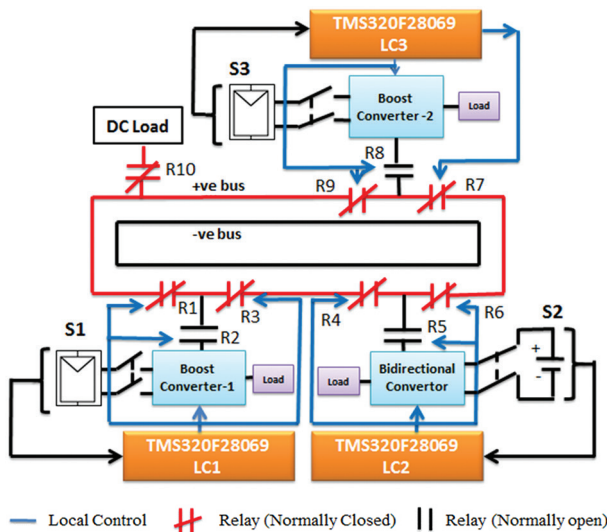


**Fig. 11.** Designed model of LVDC Microgrid

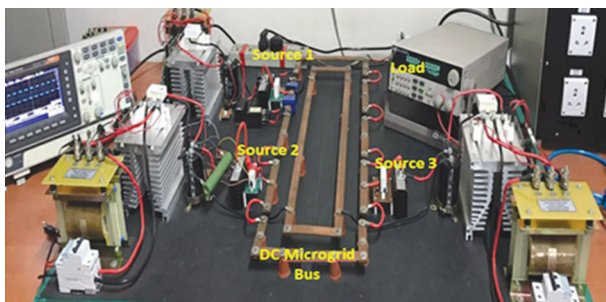


**Fig. 12.** Photograph of laboratory prototype of the DC microgrid

**Table 2.** Hardware and simulation parameters used to design dc microgrid

Parameters	Specifications
DC grid voltage	48V
Segment Resistance	10 m $\Omega$ / Km
Segment Inductance	100 $\mu$ H / Km
Segment Length	1 Km
Boost and Bidirectional converter Parameter	Power - 1000W
	Operating frequency - 20KHz
	Switch and Diode -100A, 600V IGBT module

The system consists of two Renewable Energy Sources (RES), a lead-acid battery bank, and a DC load. Each component of hardware is designed and developed in the same way as the simulation model explained in figure 2. The parameters of the designed converters are shown in Table II. Texas Instruments' TMS320F28069 digital signal processor (DSP) processor is utilized to execute control for converters and switches. Resistive attenuators are used for voltage sensing from the bus nodes. The current is sensed by the hall-effect current sensors (LEM, CTG-FBC, 50A, and 100A). The noise from the measured signal is filtered by passing it through an RC Low Pass filter and fed to the ADC to the sampling of the Digital Signal Processors (DSP's) [27-28]. Source 2 works in voltage control mode to maintain the DC bus voltage, and other sources work in current control mode to share the load current. The DSP of respective sources acts as a local controller for each source. It takes feedback from the sensing circuit and the voltage or current control mode is accomplished. Power switches (R1-R9) are integrated in the microgrid structure to isolate faulty parts under the fault condition. Power electronic load is used as DC load and is connected through a power switch R10 as shown in figure 11. Each converter connected with an appropriate power resistor working as a local load. The experiment setup is shown in figure 12.

## 6. HARDWARE RESULTS

To assess the performance of hardware it is operated under different circumstances. The suggested protection technique is implemented and verified for the bus to bus and high impedance short circuit faults. All the three sources and loading conditions decide the fault current level of the system. The major challenge in Low voltage DC microgrid is the low fault current level under no grid connectivity condition.

### 6.1 PROTECTION SCHEME OPERATION UNDER DIRECT SHORT CIRCUIT FAULT

To check the proposed algorithm, a bus to bus fault is initialized at segment 1 of the microgrid at 700 meters from the source. All the sources operated with limited capacity to ensure the safety of switches. As the fault

occurred at segment 1, a drop in converter output voltage, a drop in DC bus voltage and rise in load current is observed as shown in Figure 13. The faulty segment is separated by power switches within 150 $\mu$ s and from the calculated energy, it is identified that fault is occurs at 700 meters from the source in the segment.

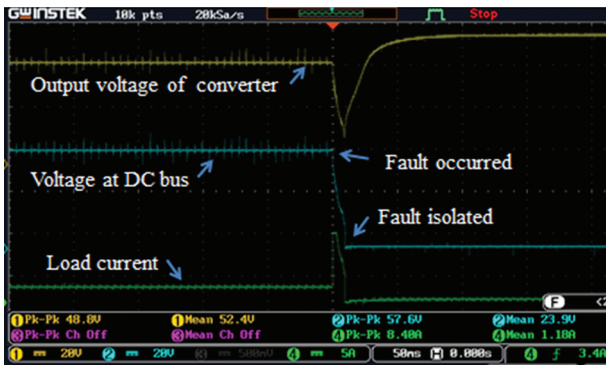


**Fig. 13.** Converter output voltage, DC bus voltage and Load current when fault occurred in segment 1.

To observe the *CumSum* and wavelet response of hardware result under the bus to bus and high impedance faults, the fault signal is stored into a CSV file from a digital storage oscilloscope and is fed to MATLAB code. Figure 14 shows the results of fault current, its calculated *CumSum*, and wavelet coefficient of fault current under bus to bus fault of segment1. Fault current has high absolute values of 14 amp with a very high rate of change in 0.4 msec.

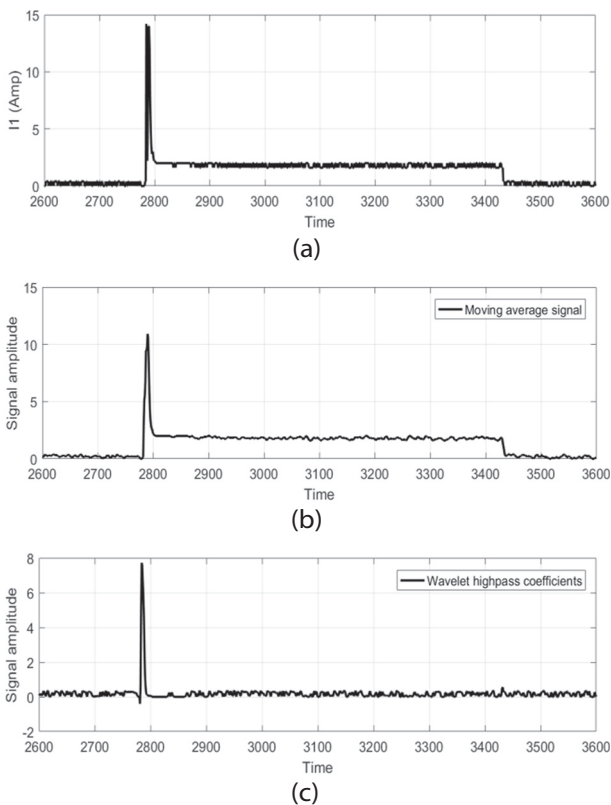


**Fig. 14.** (a) Bus to bus fault current at segment 1 (b) *CumSum* of fault current (c) Wavelet coefficients of fault current.

## 6.2 PROTECTION SCHEME OPERATION UNDER HIGH IMPEDANCE FAULT

The scheme is checked for the high impedance fault by inserting fault resistance 1 $\Omega$  in the fault path and keeping other working conditions and fault location same as previous case. The insertion of fault resistance restricts the peak value to 2.8 amp and it takes 0.4 msec. Figure 15 (a) shows the segment 1 fault current, this signal has noise due to the effect of measuring devices and the communication channels used in the system. Cumulative summation of signal in a moving average window acts like a low pass filter which does not affect the slow rise noise in the fault signal (figure 15 (b)). Also, the wavelet transform used high frequency transient to detect the fault (figure 15(c)). Hence the suggested protection technique likewise works even in a noisy environment.

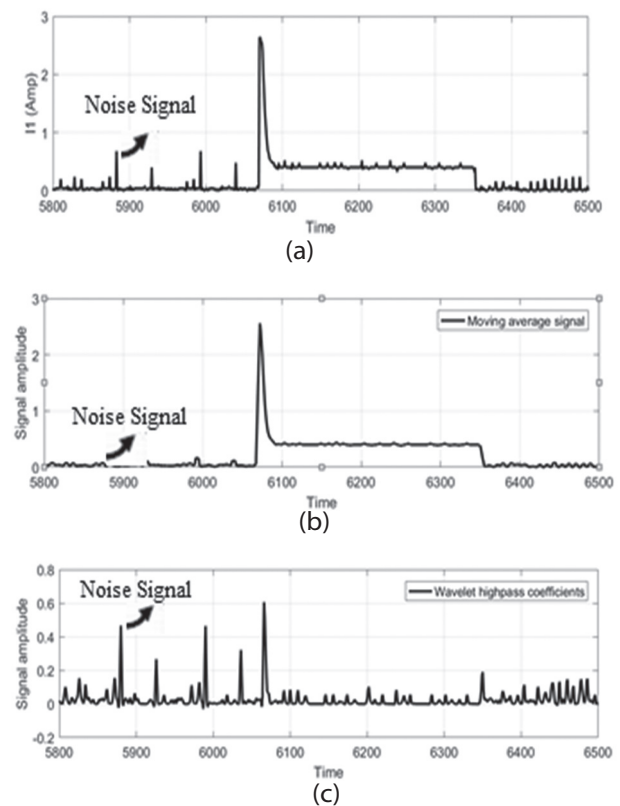


**Fig. 15.** (a) High impedance fault current at segment 1 (b) *CumSum* of fault current (c) Wavelet coefficient of fault current.

## 7. SIMULATION RESULTS

The hardware shown in figure 11 is modelled in MATLAB (Figure 2) to verify the feasibility of the algorithm under different fault conditions. The simulation parameters used for modelling are given in Table II.

The system is first simulated without fault condition by considering 1000 W load at nominal load voltage 100 volt. Both the SPV Sources S1, and S3 are contributing 81.42 W and 49.80 W is contributed by battery Source 2. Under normal operation, the source S1 and S3 are sup-

plying the major load. When the load on the microgrid is slightly increased, source S2 start sharing the increased load on the microgrid, bus voltage dips slightly for the period of overload. Figure 16 shows all four segment currents under normal operating conditions.

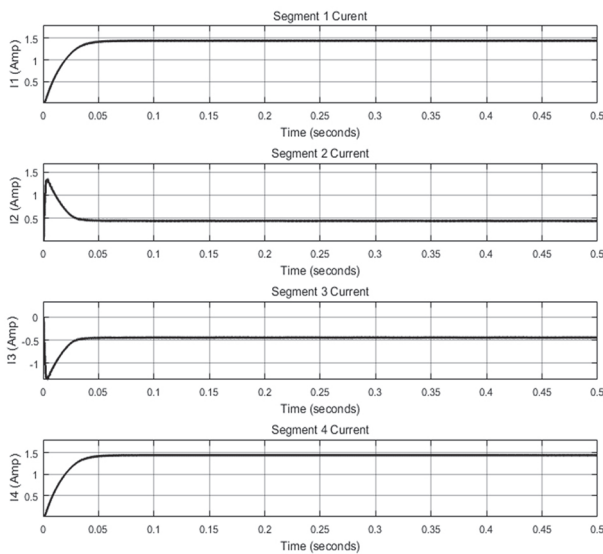


**Fig. 16.** Segment currents under normal condition

### 7.1 PROTECTION SCHEME OPERATION UNDER DIRECT SHORT CIRCUIT FAULT

The model is tested for the bus to bus fault in segment 1 at 500 meters shown in figure 17 at 0.2 sec without source limitation. The current raises 120A within 0.5 msec. Due to bus to bus short circuit, high currents transient appear in all the segments (Figure 2). Within a few milliseconds of the fault occurrence, the bus voltage decreases to zero. The segment currents are continuously measured and compared with the threshold. As the fault current exceeds the pre-set value of the calculated wavelet coefficients and the *CumSum* the protection algorithm generates a trip signal to detach the line, as shown in figure 17 (d).

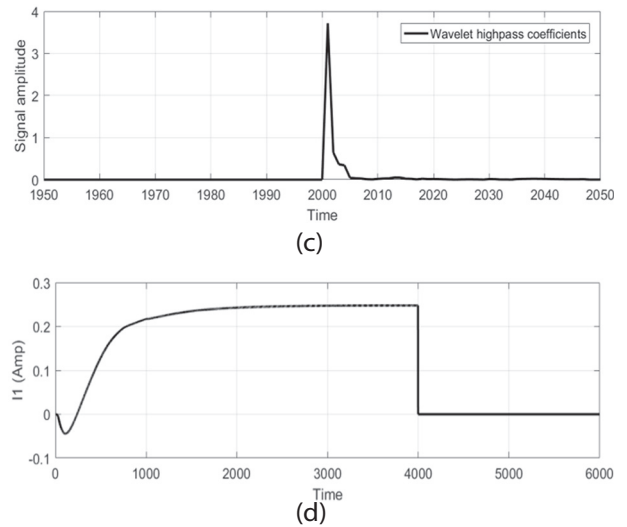
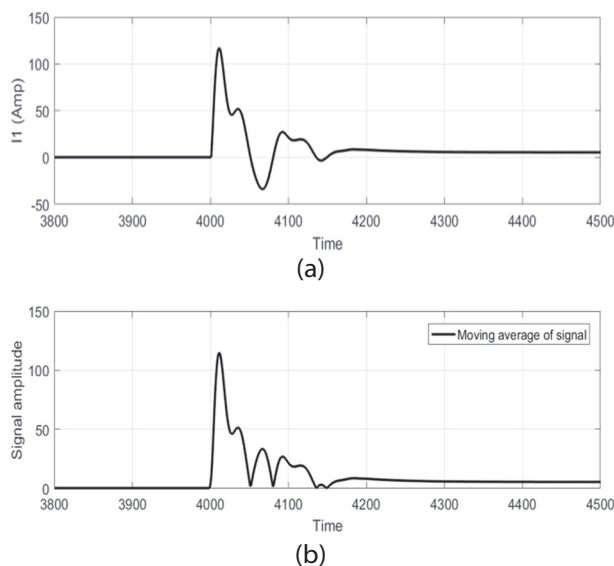
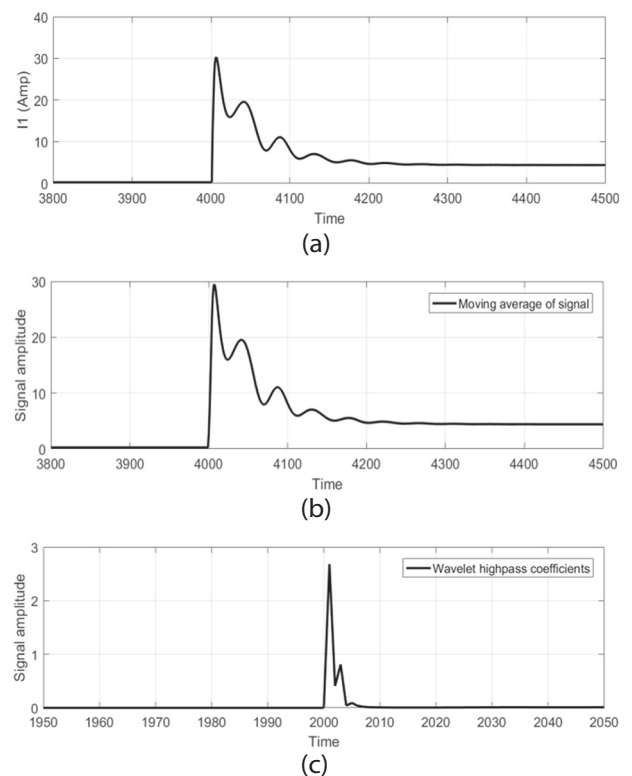


**Fig. 17.** (a) Segment 1 current due to bus to bus Fault (b) *CumSum* of fault current of segment 1 (c) Wavelet Coefficients of fault current of segment 1 (d) Segment 1 current after detection of fault.

The direct bus to bus fault is detected within 150 $\mu$ s, which guarantees the life of converters and other framework parts are ensured. The DC bus voltage immediately drops to zero on account of the excessive rate of rise of fault current.

### 7.2 PROTECTION SCHEME OPERATION UNDER HIGH IMPEDANCE FAULT

The system is tested for high impedance faults by inserting resistance  $R_F = 1\Omega$  in the fault path by keeping operating conditions and location of the fault stay the same as in the past case.



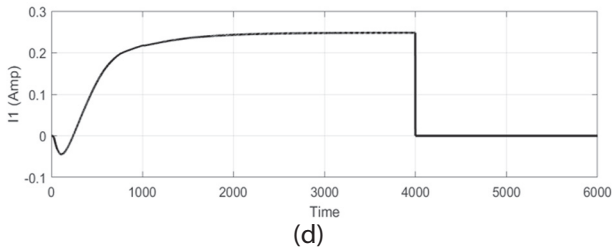


**Fig. 18.** (a) Segment 1 current due to high impedance Fault (b) *CumSum* of fault current of segment 1 (c) Wavelet of fault current of segment 1 (d) Segment 1 current before and after fault clearing.

In this case, the time taken to detect the fault is independent of the fault impedance. The fault is cleared by power switches within 150 $\mu$ s.

### 7.3 FAULT LOCALISATION IN THE SEGMENT

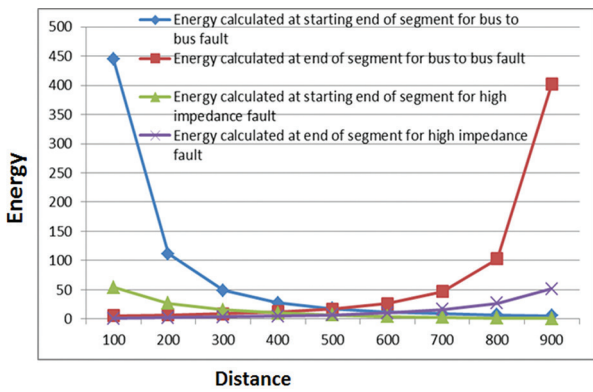


**Fig. 19.** Energy concentration vs distance in faulty segment due to bus to bus fault and high impedance fault

To check the effectiveness of algorithm for fault location identification faults are initialized after every 100m in each segment from the starting point to the end of the segment. Current is being measured at both the end of the segment and the change in energy is calculated from the wavelet high pass coefficient. The calculated energy from the starting of segment 2 to the endpoint of segment 2 for the bus to bus fault and high impedance fault is shown in figure 19, after initializing the fault in segment 2. If a bus to bus fault occurred at a point 100m from the starting point of segment 2, energy value is 450 J at starting point and 6 J at the end of segment 2. For the bus to bus fault at a point 900 m from the endpoint of segment 2 has energy value 400 J at the endpoint and 5 J at starting point of segment 2. Similarly, a change in energy values can be observed for high impedance faults. The graph is plotted for the wavelet energy changes concerning the distance in meters for segment 2. This change of energy is utilized to distinguish the location of the fault.

The developed simulation model is tested with other fault detection methods like differential fault current, over current, di/dt, and wavelet transform. Figure 20

shows the comparison of the proposed method with other fault detection methods in terms of selectivity, reliability, and accuracy. The accuracy is the ratio of number trail in which fault detect correctly to total number of trails. Selectivity is the property of protection scheme to respond to faulty zone and not others. Reliability of protection scheme is to performing its function adequately for the intended period of time under specified operating conditions. The comparison shows that the proposed method gives an accuracy of 98.72%, whereas the accuracy achieved by other methods are Wavelet transform of 92.43%, di/dt of 90.12%, overcurrent protection of 80.44%, and differential protection, 88.25%. Figure 20 also shows proposed method comparatively has the highest reliability of 99.01% and selectivity of 96.08%.

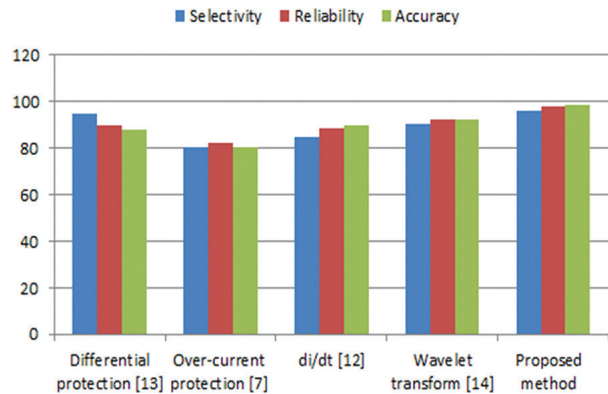


**Fig. 20.** Selectivity, reliability and accuracy comparison of the proposed method with other methods

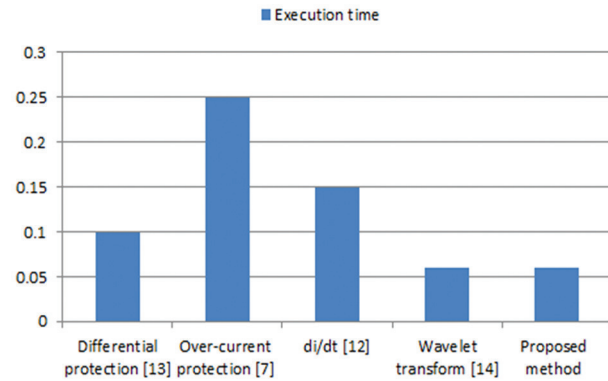


**Fig. 21.** Comparison of Execution time of the proposed method with other methods

Figure 21 shows the comparison of the proposed method with the other methods in terms of execution time. It shows that the proposed method takes lesser time to execute than wavelet transform, di/dt, overcurrent protection, and differential protection. Furthermore, the proposed method has a high sensitivity to high impedance fault comparatively overcurrent and non-unit protection method. The proposed technique does not have to rely on communication between protective relays on both sides of the protected zone for

fault detection as differential protection. The artificial neural network-based method uses two networks for fault detection and fault localization and has a complex classifier structure which leads to long training and detection time. Comparatively, the proposed method has high intelligent fault detection capability, robust and very fast selective fault isolation capability.

## 8. CONCLUSION

An efficient protection scheme using *CumSum* and Wavelet transform is proposed and implemented in a Ring-type LVDC microgrid system. The fault is being detected from the fault current average using *CumSum* and fault features extracted using Wavelet transform. Depending on the severity of the fault, the *CumSum* of even a healthy section crosses the set threshold value which may lead to the maloperation of the healthy system. However, the Wavelet transform can identify the faulty segment irrespective of the severity and location of the fault. During sudden changes in load, *CumSum* value is not changing much whereas wavelet coefficient goes above the set threshold value, indicating even load change as a fault. The hybrid model works well under fault conditions and dynamic conditions and can distinguish between dynamic operation and a fault in the DC microgrid. The threshold values for *CumSum* and Wavelet transform are calculated analytically and the same is used in the algorithm. Energy per cycle is determined from the wavelet coefficient and is used to find the fault location, accordingly taking out the requirement for additional hardware to distinguish the fault area. From the comparative study, it is shown that the proposed method has higher accuracy 98.72%, higher selectivity 96.08%, higher reliability 99.01%, and lower execution rate in comparison with the existing fault detection methods in the discrimination of fault and system dynamic situations. The proposed methodology is robust, highly sensitive to high impedance fault, does not require communication between protection devices, and has fast selective fault isolation capability. The research can be additionally extended to optimum load sharing and stability study. The methodology will be more advantageous if it can handle system dynamics to maintain the stability of the system from the span of occurrence of fault to its isolation. A more detailed control approach can be evolved to make the system stable and reliable.

## 9. REFERENCES

- [1] Y. Ito, Z. Yang, A. Hirofumi, "DC microgrid based distribution power generation system", Proceedings of the 4<sup>th</sup> International Power Electronics and Motion Control Conference, 2004.
- [2] S. Augustine et al. "DC Microgrid Protection: Review and Challenges", Technical report, Sandia National Laboratory, Albuquerque, NM, USA, 2018.
- [3] A. Chandra, G. K. Singh, V. Pant, "Protection techniques for DC microgrid-A review", Electric Power Systems Research, Vol. 187, 2020, p. 106439.
- [4] S. Som, S. R. Samantaray, "Efficient protection scheme for low-voltage DC micro-grid", IET Generation, Transmission & Distribution, Vol.12, No. 13, 2018, pp. 3322-3329.
- [5] D. Kumar, F. Zare, A. Ghosh, "DC microgrid technology: system architectures, AC grid interfaces, grounding schemes, power quality, communication networks, applications, and standardizations aspects", IEEE Access, Vol. 5, 2017, pp. 12230-12256.
- [6] R. Kamel, K. Nagasaka, "Effect of load type on standalone micro grid fault performance", Applied energy, Vol. 160, 2015, pp. 532-540.
- [7] P. Mahat et al. "A simple adaptive overcurrent protection of distribution systems with distributed generation", IEEE Transactions on Smart Grid, Vol. 2, No. 3, 2011, pp. 428-437.
- [8] R. Mohanty, S. M. Balaji, A. K. Pradhan, "An accurate noniterative fault-location technique for low-voltage DC microgrid", IEEE Transactions on Power Delivery, Vol. 31, No. 2, 2015, pp. 475-481.
- [9] J. Wang et al. "Fast fault selection and location for a marine power system using system power converters, and active impedance estimation", Proceedings of the 4<sup>th</sup> IET Conference on Power Electronics, Machines and Drives, 2008.
- [10] F. Wilches-Bernal et al. "A Survey of Traveling Wave Protection Schemes in Electric Power Systems", IEEE Access, Vol. 9, 2021, pp. 72949-72969.
- [11] S. S. Balasreedharan, S. Thangavel, "An adaptive fault identification scheme for DC microgrid using event based classification", Proceedings of the 3rd International Conference on Advanced Computing and Communication Systems, 2016.
- [12] A. Meghwani, S. Srivastava, S. Chakrabarti, "A new protection scheme for DC microgrid using line current derivative", Proceedings of the IEEE/PES General Meeting, 2015, pp.1-5.
- [13] D. Salomonsson, L. Soder, A. Sannino, "Protection of low-voltage DC microgrids", IEEE Transactions on Power Delivery, Vol. 24, No. 3, 2009, p. 1045.

- [14] D. K. J. S. Jayamaha, N. W. A. Lidula, A. D. Rajapakse, "Wavelet-multi resolution analysis based ANN architecture for fault detection and localization in DC microgrids", *IEEE Access*, Vol. 7, 2019, pp. 145371-145384.
- [15] D. Patil, S. Bindu, S. Thale, "Deep neural network enable fault detecting in LVDC microgrid using empirical mode decomposition", *International Journal of Advance Technology and Engineering Exploration*, Vol. 9, No. 87, 2022; pp. 200-215.
- [16] J.-D. Park, J. Candelaria, "Fault detection and isolation in low-voltage DC-bus microgrid system", *IEEE transactions on power delivery*, Vol. 28, No. 2, 2013, pp. 779-787.
- [17] Y. Wang, Z. Zhang, Y. Fu, Y. Hei, X. Zhang, "Pole-to-ground fault analysis in transmission line of DC grids based on VSC", *Proceedings of the IEEE 8th International Power Electronics and Motion Control Conference*, 2016.
- [18] A. Meghwani, S. C. Srivastava, S. Chakrabarti, "A non-unit protection scheme for DC microgrid based on local measurements", *IEEE Transactions on Power Delivery*, Vol. 32, No. 1, 2016, pp. 172-181.
- [19] S. Fletcher et al. "High-speed differential protection for smart DC distribution systems", *IEEE Transactions on Smart Grid*, Vol. 5, No. 5, 2014, pp. 2610-2617.
- [20] D. Patil, S. Bindu, "Real time protection technique for DC microgrid using local measurements", *Proceedings of the Technologies for Smart-City Energy Security and Power Conference*, 2018.
- [21] S. Beheshtaein et al. "DC microgrid protection: A comprehensive review", *IEEE Journal of Emerging and Selected Topics in Power Electronics*, 2019. (in Press)
- [22] R. Polikar, "The Wavelet Tutorial Second Edition Part I", <https://ccrma.stanford.edu/~unjung/mylec/WTpart1.html> (accessed: 2021)
- [23] D. Obertson, O. Camps, J. Mayer, W. Gish, "Wavelets and electromagnetic power system transients", *IEEE Transactions on Power Delivery*, Vol. 11, No. 2, 1996, pp. 1050-1058
- [24] D. Patil, G. Pushkar, V. Patwardhan, M. Gadre, "On the design of FIR wavelet filter banks using factorization of a halfband polynomial", *IEEE Signal Processing Letters*, Vol. 15, 2008, pp. 485-488.
- [25] K. De Kerf et al. "Wavelet-based protection strategy for DC faults in multi-terminal VSC HVDC systems", *IET Generation, Transmission & Distribution*, Vol. 5, No. 4, 2011, pp. 496-503.
- [26] U. Maqbool, U. A. Khan, "Wavelet Based Feature Analysis of Fault Signals in a Microgrid", *Proceedings of the International Conference on Power Generation Systems and Renewable Energy Technologies*, 2018.
- [27] J.-D. Park, J. Candelaria, L. Ma, K. Dunn, "DC ring-bus microgrid fault protection and identification of fault location", *IEEE transactions on Power delivery*, Vol. 28, No. 4, 2013, pp. 2574-2584.
- [28] C. Patil et al. "A novel protection scheme for DC microgrid with hierarchical control", *Proceedings of the IEEE International Conference on Smart Energy Grid Engineering*, 2017.